Growth directions of microstructures in directional solidification of crystalline materials

J. Deschamps, M. Georgelin, and A. Pocheau
IRPHE, Aix-Marseille Universités, CNRS, 49 rue Joliot-Curie, B.P. 146, Technopôle de Château-Gombert, F-13384 Marseille, Cedex 13, France

(Received 29 January 2008; revised manuscript received 20 May 2008; published 30 July 2008)

In directional solidification, as the solidification velocity increases, the growth direction of cells or dendrites rotates from the direction of the thermal gradient to that of a preferred cristalline orientation. Meanwhile, their morphology varies with important implications for microsegregation. Here, we experimentally document the growth directions of these microstructures in a succinonitrile alloy in the whole accessible range of directions, velocities, and spacings. For this, we use a thin sample made of a single crystal on which the direction of the thermal gradient can be changed. This allows a fine monitoring of the misorientation angle between thermal gradient and preferred crystalline orientation. Data analysis shows evidence of an internal symmetry which traces back to a scale invariance of growth directions with respect to a Péclet number. This enables the identification of the relationship between growth directions and relevant variables, in fair agreement with experiment. Noticeable variations of growth directions with misorientation angles are evidenced and linked to a single parameter.

DOI: 10.1103/PhysRevE.78.011605 PACS number(s): 81.10.Aj, 81.30.Fb, 68.70.+w

I. INTRODUCTION

Casting stands as a canonical manufacturing process for solidifying melt alloys into ingots or materials of prescribed forms. In this latter case, it consists in introducing a melt into a mold of suitable form and in letting it progressively freeze from the boundaries. Meanwhile, a solidification front advances into the melt, together with the melting isotherm. This, possibly supplemented with spontaneous germinations of solid within the melt bulk, eventually yields the complete solidification of the material inside prescribed boundaries. This process appears especially useful to provide materials of complex shape that would be difficult or uneconomical to obtain by other methods. It inherently involves thermal gradient and is thus relevant to directional solidification.

Casting, however, generates various heterogeneities on a large range of scales. They correspond, at the submillimeter scale, to the modulations of solute concentration induced by dendritic microstructures (microsegregation [1]); at the millimeter scale, to the abrupt change of dendrite orientation from grain to grain; at the centimer scale and beyond, to dendrites growing normally to the mold boundaries (so-called columnar zone) or displaying, farther in the bulk, fuzzy orientations due to spontaneous germinations (so-called equiaxed zone). Dendrite orientations thus appear mostly dictated by thermal gradient in the columnar zone and by crystal orientation in the equiaxed zone. However, in most parts of the material, they actually depend on *both*, in a way which sensitively drives microstructure morphologies with important implications on the physical properties of the cast object.

The dependence of microstructure orientations to those of the thermal gradient and the crystal lattice originates from the fact that, when the solidification velocity increases, the growth direction of dendrites *rotates* from the thermal gradient direction $\mathbf{G}$ to a definite direction $\mathbf{a}$ prescribed by the crystal orientation [1–7]. The issue then consists in accurately determining this rotation law at all misorientation angles $\Theta_0=(\mathbf{a},\mathbf{G})$ and in providing insights into the underlying physical phenomena. This calls for going beyond the classical directional configuration where the thermal gradient is aligned onto a principal cristalline axis.

Surprisingly, although the variation of the growth direction of dendrites has been qualitatively noticed in the literature [1,2], few quantitative studies have been devoted to it. In particular, to our knowledge, no theory of it is available in the nonlinear regime. Three experiments [3–5] and two numerical simulations [5,6] have provided data on dendrite growth directions, but two of them omitted to report on an essential variable: the dendrite spacing [3,4]. The remaining studies evidenced, for two angles Θ_0, a collapse of data on curves $\Theta(\Theta_0,\mathrm{Pe})$ relating the growth direction angle Θ to a Péclet number Pe [5]. However, the number of misorientation angles investigated was not large enough to provide an explicit determination of the growth direction law of dendrites [5,6]. In contrast, their data evolution shows an intricate coupling between Θ, Pe, and Θ_0 which calls for a complete investigation of the *whole* (Θ_0,Pe) space to be appropriately characterized.

The purpose of this study is to perform an exhaustive experimental investigation of the way microstructures change growth direction and morphology when their solidification velocity, their spacing, and the misorientation angle between thermal gradient and crystal lattice vary. This is achieved with a large accuracy on a large amount of data by varying the thermal gradient direction on thin samples of single crystals of a succinonitrile-based alloy. The resulting data library provides the first experimental determination of growth directions of microstructures in the full range of misorientation angles between crystal lattice and heat flow. It enables the main nonlinear evolutions and internal couplings to be clarified in the whole accessible variable space. In particular, a hidden symmetry—a Péclet scale invariance—is evidenced and exploited. Interestingly, it enables the form of the relationship governing dendrite growth directions to be determined up to an exponent and a prefactor that are eventually fixed from the data library. This provides the first ana-

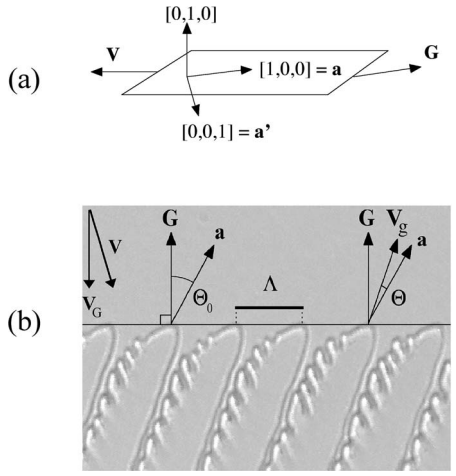

FIG. 1. Main variables. (a) Directions of the principal crystalline axes with respect to the sample plane. One axis is normal to the plane. The closest axis to **G** in the plane is labeled **a**. It corresponds to the growth direction of large velocity dendrites and is called preferred crystalline direction. (b) Characteristic variables: growth velocity $\mathbf{V}_g$, thermal gradient **G**, preferred crystalline direction **a**, and dendrite spacing Λ. Only the projection $\mathbf{V}_G$ of the pushing velocity **V** on the direction of **G** matters for solidification here. It is called the solidification velocity.

lytic identification of the evolution of growth directions with the relevant variables. Altogether, these results provide a stimulating insight for theoretical investigation and a useful parametrization for developing practical models of microstructure formation in cast materials.

The article is organized as follows. Section II reports the main issue, its modeling, and the results obtained so far in the literature. The experimental setup, the methods, and the procedures applied in the study are detailed in Sec. III. The qualitative results regarding the growth direction, the morphology, and the stability of microstructures are reported in Sec. IV. Section V is then devoted to an analysis of data, to the evidence of their scale invariance with respect to the Péclet number, and to the identification of the growth direction law. A discussion of these results, a comparison with the literature, and a conclusion about this study follow.

II. INTERFACIAL ANISOTROPY AND GROWTH DIRECTION

We report the implications of interfacial anisotropy on microstructure growth directions, define the variables and the objectives of the study, and recall the previous works devoted to this issue in the literature.

A. Growth directions in solidification

We define the growth velocity $\mathbf{V}_g$ of a microstructure as the velocity of one of its characteristic points, usually its tip, with respect to the surrounding liquid phase [Fig. 1(b)]. The direction of $\mathbf{V}_g$ then provides the microstructure growth direction.

In free growth—i.e., at vanishing thermal gradient—the only characteristic directions of the medium are the crystal axes. They then naturally drive the growth directions of dendrites which are usually aligned on crystal axes of high symmetry. However, depending on the balance between stiffness and kinetic interfacial anisotropy, intermediate directions may be preferred [8].

In directional solidification, an additional direction is brought about by the thermal gradient **G**. A competition with the crystal orientation then sets in for prescribing the microstructure growth directions. As a result, these directions stand in between that of **G** and that which would have been displayed in free growth. In particular, as the solidification velocity rises, the dendrite growth directions are found to rotate from the direction of **G** to a definite asymptotical direction prescribed by the crystal orientation [2–7] and labeled **a** in the following [Fig. 1(b)].

The origin of the link between crystal anisotropy and solidification interface stems from the Gibbs-Thomson relationship

$$T_I = T_M + mc_I - \frac{T_M}{Q}\left(\frac{\tau_1}{R_1} + \frac{\tau_2}{R_2}\right) - \beta V_I.$$

This relation expresses the interface temperature T_I in terms of the melting temperature T_M, the solutal concentration at the interface c_I, a capillary correction involving the principal curvature radii R_j, $j=1,2$, and a kinetic correction involving the interface velocity V_I. Here, Q denotes the volumic latent heat, m the liquidus slope, τ_j, $j=1,2$, the interfacial stiffnesses, and β a kinetic factor. It then appears that both τ_j and β slightly depend on the angles $\theta_i=(\mathbf{a}_i,\mathbf{n})$ of the interface normal **n** with respect to the crystal axes $\mathbf{a}_i$. In particular, on a cubic crystal, $\tau_j(\mathbf{n})=\gamma_0[1-\epsilon_c f_4(\mathbf{n})]+o(\epsilon_c)$ and $\beta(\mathbf{n})=\beta_0[1-\epsilon_k f_4(\mathbf{n})]+o(\epsilon_k)$, with $f_4(\mathbf{n})=\cos(4\theta_1)$, when a crystal axis is, as in our experiment, normal to the sample plane [Fig. 1(a)].

This orientational modulation of the interface temperature then proves to significantly influence microstructure forms and growth directions. This is actually surprising in view of the extreme weakness of the anisotropic modulations. In particular, in the material used here, succinonitrile (SCN), the interface temperature is only modulated by 6 mK at most, a value which corresponds in the actual thermal gradient G of 140 K cm^{-1} to a modulation of interface position of at most 40 nm. However, this nevertheless succeeds in prescribing, at large solidification velocity, the growth direction of dendrites, despite their much larger scale of a hundred micrometers.

B. Variables and main issues

The variables of the system correspond to the mixture properties $(D,m,k,c_\infty,d_0,\beta_0,\epsilon_c,\epsilon_k)$, to the imposed conditions $(\mathbf{G},\mathbf{V})$, to microstructure features (Λ), and to the crystal orientation (Θ_0). The former variables refer to the solutal diffusivity D, the liquidus slope m, the partition coefficient k, the solutal concentration of the melt c_∞, the capillary length $d_0=\gamma_0 T_M/Q$, the kinetic coefficient β_0 and the anisotropy coefficients ϵ_c and ϵ_k. The imposed growth conditions correspond to the thermal gradient **G** and to the pushing velocity **V** of the liquid phase in the thermal gradient frame (Fig. 2).

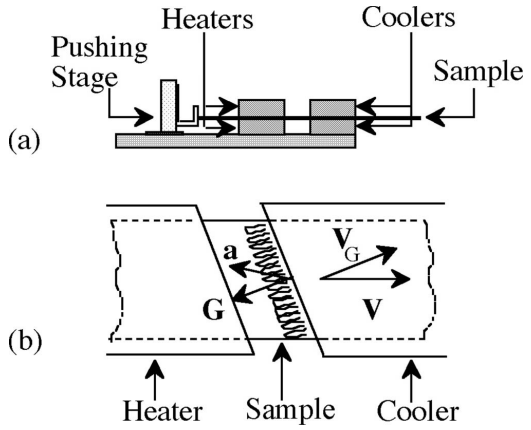

FIG. 2. Sketch of the experimental setup. (a) Side view. The sample is pushed at a prescribed velocity $\mathbf{V}$ in a controlled thermal gradient $\mathbf{G}$. (b) Top view. The thermal gradient direction is monitored by the thermal boundaries orientation. This enables its angle with a preferred crystalline direction $\mathbf{a}$ to be routinely changed. The relevant pushing velocity for solidification is the projection $\mathbf{V}_G$ of $\mathbf{V}$ on the direction $\mathbf{G}$.

The microstructure features reduce here to their spacing Λ defined as the distance between their tips [Fig. 1(b)].

To specify the crystal orientation, we note that we shall use a body-centered crystal (SCN), a sample thin enough for yielding a single microstructure layer and a single crystal with a principal axis normal to the sample plane [Fig. 1(a), Sec. III B]. Accordingly, crystal orientation will only exhibit one rotational degree of freedom representable by a vector in a plane. This will allow to use the asymptotic direction $\mathbf{a}$ to fully represent the crystal orientation by the angle $\Theta_0 = (\mathbf{a}, \mathbf{G})$ it makes with the thermal gradient [Fig. 1(b)]. Similarly, the growth direction of microstructures will be characterized by the angle $\Theta = (\mathbf{a}, \mathbf{V}_g)$ made by the asymptotic direction $\mathbf{a}$ with the growth velocity $\mathbf{V}_g$ [Fig. 1(b)].

Whereas the mixture properties are fixed in the whole study, the amplitude of V and Λ and the direction of $\mathbf{G}$ will be varied. The value of V is directly monitored from the setup and the direction of $\mathbf{G}$ will be rotated by acting on the thermal devices (Fig. 2). Finally, the dendrite spacing Λ will be changed by managing the growth history and by considering different parts of the interface.

In contrast with usual directional solidification setups [3–5,9,10], the one we use displays a pushing velocity $\mathbf{V}$ not aligned with the thermal gradient $\mathbf{G}$ [Fig. 2(b)]. However, the velocity component *normal* to $\mathbf{G}$ only makes the sample glide along isothermal lines. It has thus no physical consequence and will be skipped in the following. It then remains the velocity component *parallel* to the $\mathbf{G}$, $V_G = |\mathbf{V} \cdot \mathbf{G}| / G$, which drives the rate at which material points change temperature [Fig. 1(b)]. This effective pushing velocity corresponds to the velocity which actually matters regarding solidification. From now on, we shall therefore use it as the relevant solidification velocity.

Our main issue will then consist in determining how, in directional solidification, the growth direction of microstructures rotates from the direction $\mathbf{G}$ to the direction $\mathbf{a}$ as the relevant variables change. It will call for the following achievements: (i) experimentally determine the growth directions of microstructures at various angles Θ_0, solidification velocities V_G, and spacings Λ; (ii) express their variations by a definite relationship; and (iii) point out the physical properties attached to it. Quantitatively, this will call for determining the relationship $\Theta = f(\Theta_0, V_G, \Lambda)$, the other variables of the system being taken as constant here.

C. Former quantitative studies

To our knowledge, the sole theoretical studies refer to the generation of drift sinusoidal waves [11] or of tilted cells [12] by kinetic anisotropy in a linear [11] or weakly nonlinear [12] analysis of interface dynamics. On the other hand, three experiments [3–5] and two numerical simulations [5,6] only have quantitatively analyzed dendrite growth directions on plastic materials [3–5] or on steel [6].

The experiment and the simulation reported in [5] revealed a dependence of the tilt angle of dendrites on the Péclet number $\mathrm{Pe} = \Lambda V_G / D$. In contrast, two previous experiments did not report on the dendrite spacing Λ, so that their data scattering or evolution suffered from this indeterminacy [3,4]. The curves $\Theta(\Theta_0, \mathrm{Pe})$ evidenced in [5,6] differed depending on the misorientation angle $\Theta_0 = (\mathbf{a}, \mathbf{G})$. However, the number of misorientation angles studied—two numerically (17° [6] and 30° [5]) and two experimentally ($32 \pm 2°$ and $40 \pm 2°$ [5])—was too low to allow an explicit determination of the relation $\Theta(\Theta_0, \mathrm{Pe})$ and a detailed investigation of the way these curves vary with Θ_0. Nevertheless, numerical simulations at fixed Pe evidenced a nonlinear evolution of Θ with Θ_0 at $\mathrm{Pe} = 2.758$ [6] and $\mathrm{Pe} = 2.925$ [5]. This nonlinearity contrasts with the linear variation of Θ with Θ_0 at low Pe implied by the alignment of $\mathbf{V}_g$ on $\mathbf{G}$ ($\Theta \approx \Theta_0$). It thus points to a nonlinear coupling between Θ_0 and Pe which calls for a systematic investigation on the whole variable space to be clarified.

This statement has motivated the present experimental study. In particular, the large amount of data obtained here will allow the quantitative determination of the growth direction law and the identification of the nature of its nonlinearity with respect to the Péclet number Pe and the misorientation angle Θ_0.

III. EXPERIMENTAL SETUP AND METHODS

We report the experimental setup and the procedures used to determine microstructures growth directions. Emphasis is put on the specificities required to manage the misorientation angle Θ_0 and achieve accurate measurement of growth directions.

A. Directional solidification setup

The setup is designed to provide the directional solidification, at a controlled velocity, of thin samples of a transparent material together with its direct observation by optical means [Fig. 2(a)] [10,13]. It is composed of a mechanical part which pushes a thin sample into a thermal part in which it solidifies. An optical part placed far from the solidification

setup provides a nonperturbative visualization of the growth interface.

The mechanical part is made of a microstepper motor coupled to a linear ball-screw-driven stage. The motor involves 200 steps per turn, 32 microsteps by steps, and is slowed at each microstep by Foucault current to prevent vibration. The screw involves a 5-mm thread, and the sample translation is controlled by a Michelson interferometer. This provides pushing velocities up to 50 μm s^{-1} with a relative accuracy better than $\pm 3\%$ on a thread.

The thermal part involves heaters and coolers distant from a controlled gap of several millimeters. Both are made of top and bottom blocks sandwiching the sample and electronically regulated to better than 0.1 K. Their temperatures, 100 °C and 10 °C, are set so that the solidification interface stands in between.

The sample is built by gluing together two glass plates by their sides with two bands of calibrated sheet in between. This provides a 50-μm-thick space which is next filled with the mixture to solidify. We use a nearly pure transparent plastic crystal, the succinonitrile $CNCH_2—CH_2CN$ (SCN), which provides rough solidification interfaces. NMR analysis has revealed that its dominant impurity involves an ethylenic bond, corresponding to ethylen ($CH_2=CH_2$) or cyanoethylen ($CH_2=CHCN$) also called acrylonitrile. On the other hand, no chemical bond of another kind of impurity could be detected by NMR or IR spectroscopy or by any noticeable event in this experimental study or in previous ones. This excludes in particular any presence of water which could not actually enter the mixture during the sample filling under nitrogen atmosphere. To preserve a large zone free of boundary disturbances, we took a large sample width of 45 mm. Also, to allow the study of long runs beyond transients, we took long samples of 15 cm.

The visualization of the solidification interface is achieved on a charge-coupled-device (CCD) camera from the aberrations undergone by a parallel light beam crossing the sample. An exploded optical setup with a large frontal distance is used instead of a compact microscope to ensure the absence of thermal perturbations on the interface. The camera involved 768×512 pixels, and the width of the visualized interface was usually 2 mm.

In order to make an experimental run refer to a definite misorientation angle Θ_0 between thermal gradient and crystal orientation, it is convenient to operate with a single crystal in the whole sample using the procedure reported below. The absence of grain boundaries in the sample then promoted microstructure homogeneity. In addition, we paid attention to studying the most homogeneous regions which extended on at least 20 cells or dendrites and often more. Interestingly, however, homogeneity does not mean a unique available microstructure spacing Λ at given solidification variables. Instead, depending on the solidification history—e.g., on the ramp of velocity and its implication for coarsening—a large spacing range of about a factor of 2 can be obtained [10]. As in previous studies, we used this feature to scan the system properties with respect to the microstructure spacing Λ.

The variables ranges of the experiment were the following: $D=1350\pm 50$ μm^2 s^{-1}, $k=0.29\pm 0.05$, $G=140$ K cm^{-1}, and critical velocity $V_c \approx 2.3$ μm s^{-1}. Pushing velocities and microstructure spacings varied from $V=5$ to 50 μm s^{-1} and from $\Lambda=70$ to 230 μm.

B. Single-crystal achievement

The selection of a single crystal has been achieved iteratively by a controlled solidification and fusion process performed on an auxiliary setup. There grain orientations were evidenced from the growth direction of rapidly solidifying dendrites. A grain of appropriate orientation was then selected and used as a nucleus for the solidification of the whole sample. This was achieved by heating until the whole material has fused except the selected grain and then by cooling back to complete solidification. Equiaxed grains spontaneously generated in the bulk or columnar grains grown from the sides were progressively eliminated the same way, eventually yielding a single crystal.

Interestingly, on a given sample, large velocity dendrites always grew along either a fixed direction **a** or its normal **a**′ in the sample plane [Fig. 1(a)], depending on the direction of **G**. We checked that these directions actually correspond to those displayed by the cross shape made in the same sample by freely growing germs. In addition, this cross shape displayed a fourfold symmetry and the sidebranches developed in the sample depth [10] were normal to the sample plane. This means that the sample normal was a [100] axis of the crystal [Fig. 1(a)]. This statement was supported by the existence of a degenerate mode [Figs. 4(j) and 6(c)] instead of seaweeds or doublons at a large misorientation angle $\Theta_0 \approx 45°$ [14]. It enabled us to simply characterize the crystal orientation by the angle $\Theta_0=(\mathbf{a},\mathbf{G})$ [Fig. 1(b)]. Of course, as the directions **a** and **a**′ are physically equivalent, the relevant range of variation of Θ_0 stands in between 0° and 45°. The determination of **a** was finally achieved from the growth direction of rapidly solidifying dendrites to an accuracy of 0.1°.

C. Control of thermal gradient orientation

Our issue calls for a fine control of the misorientation angle $\Theta_0=(\mathbf{a},\mathbf{G})$ in its full accessible range. Variation of Θ_0 can be obtained by turning the direction of **a**, the direction of **G**, or both. In previous experiments [3–5], **a** was varied with no direct determination of its direction and no control of an exhaustive scanning of angles Θ_0. Here, the use of a single crystal and of orientable thermal boundaries offers the opportunity to manage Θ_0 by definite rotations of either **a** or **G** with preliminary determination of both directions.

As it is much easier to monitor the rotation of a macroscopic field rather than a microscopic field, we chosed to rotate the direction of **G** on given samples—i.e., at fixed **a**—simply by rotating the boundaries of the thermal blocks that produce the thermal gradient. However, as the experimental setup does not permit to rotate the blocks with respect to the sample axis, we have chosen to prolongate them by angular extensions suitably designed for providing a rotated thermal boundary [Fig. 2(b)]. Six rotation angles of **G** in between 0 and 45° were then used on the same sample with an accuracy of 0.1°.

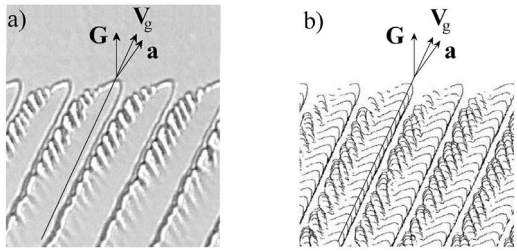

FIG. 3. Measurement of growth direction on tilted dendrites. $V=30\ \mu\mathrm{m\ s}^{-1}$. Actual interface (a) and corresponding sequential snapshots in the sample frame (b). The tip trajectory provides the growth direction $\mathbf{V}_g$. It differs from the groove orientations (a) due to continued groove solidification.

D. Growth direction measurement

The growth direction angle Θ is determined by reconstructing the dendrite tip trajectory in the sample frame. This is achieved by plotting a diagram in which the successive skelets of the solidification interface are translated on the direction of **G** of the distance they actually crossed [Fig. 3(b)]. The line joining the successive positions of a microstructure tip then provides its growth angle Θ to an accuracy of 0.1°. Notice that the tip trajectory makes few degrees with the groove direction [Fig. 3(a)], as a result of the ongoing solidification of groove.

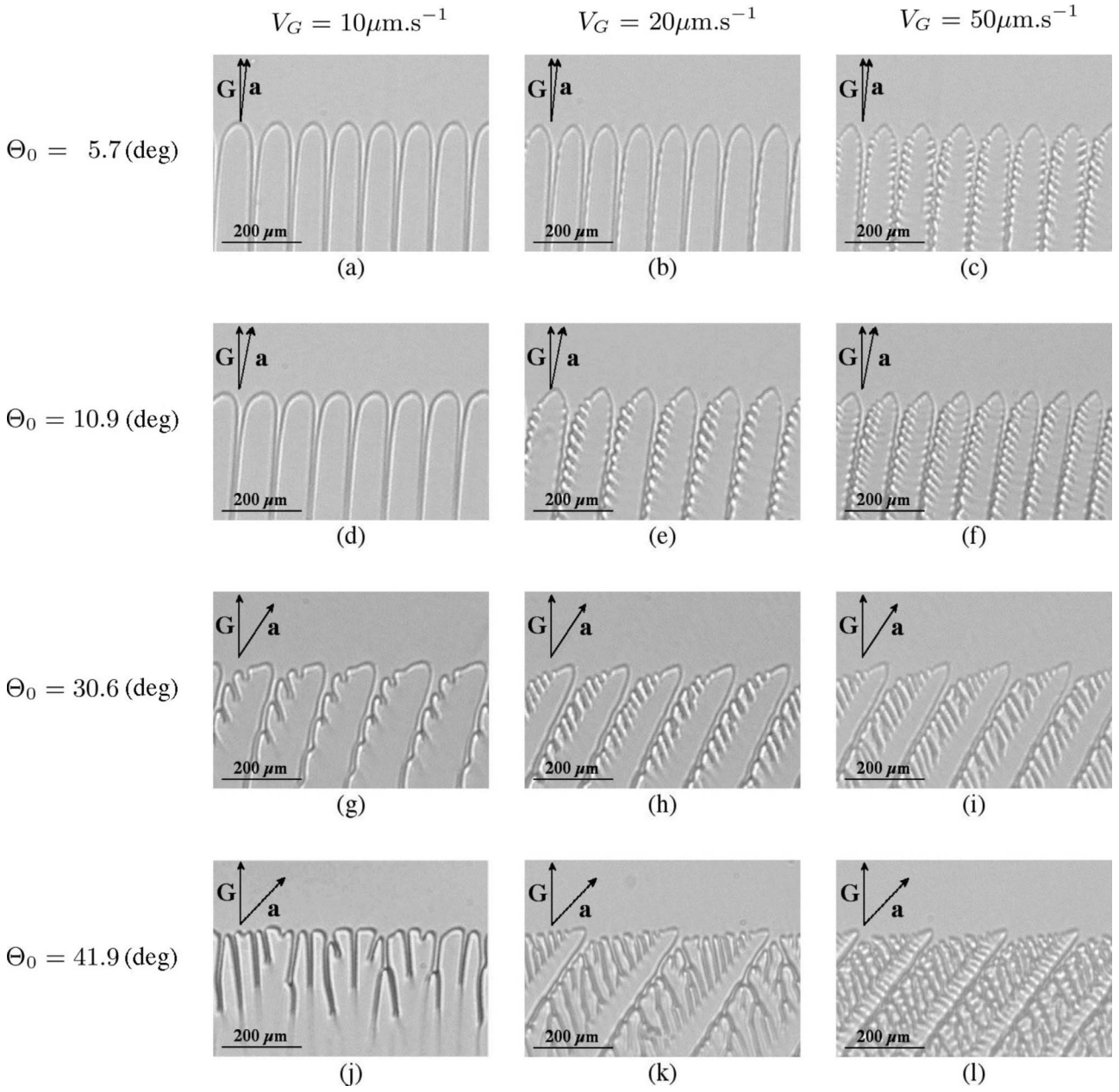

FIG. 4. Microstructure library for increasing velocity V_G (lines) or misorientation angle Θ_0 (columns).

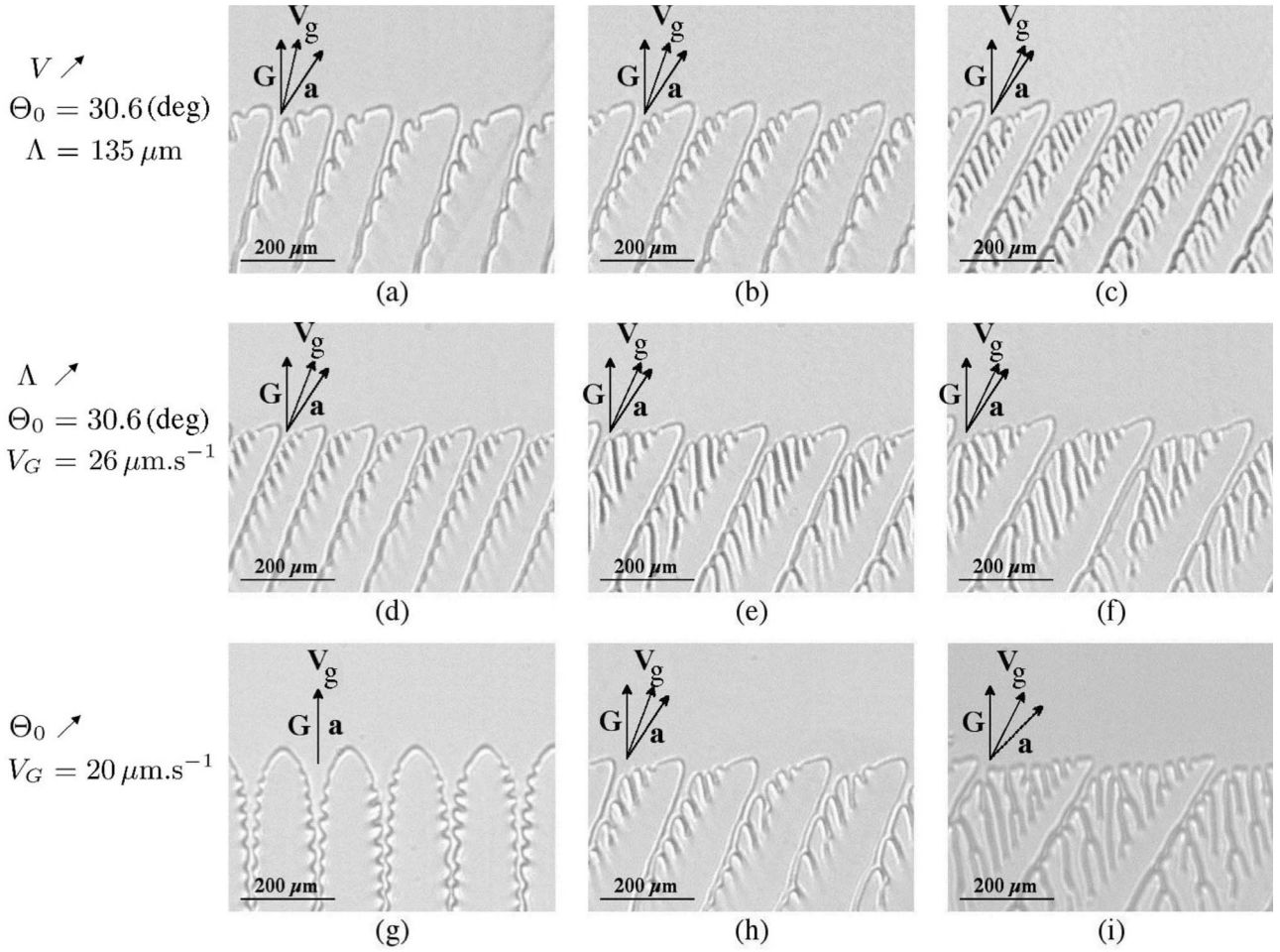

FIG. 5. Evolution of growth directions for increasing velocity V_G [(a), (b), (c)], spacing Λ [(d), (e), (f)], or misorientation angle Θ_0 [(g), (h), (i)]. (a), (b), (c) Θ_0=30.6°, Λ=135 μm, V_G (μm s^{-1})=8.7 (a), 17.3 (b), and 43.3 (c). (d), (e), (f) Θ_0=30.6°, V_G=26 μm s^{-1}, Λ(μm) =112 (d), 174 (e), and 214 (f). (g), (h), (i) V_G=20 μm s^{-1}, Θ_0(deg)=0 (g), 30.6 (h), and 41.9 (i), Λ(μm)=145 (g), 160 (h), and 213 (i).

IV. GROWTH DIRECTIONS, MORPHOLOGIES, AND INSTABILITIES

We qualitatively report the main features of the microstructure library provided by the experiment with emphasis on the evolutions of growth directions and morphologies and the occurrence of instabilities.

A. Morphologies

Figure 4 reports the morphology of cells or dendrites at various misorientation angles Θ_0 and velocities V_G. The main noticeable features are a dendrite tilting accompanied by an asymmetry of form and of sidebranch development and a transition to another kind of microstructures where growth directions fluctuate.

Dendrite tilting is all the more pronounced that V_G or Θ_0 are large. However, it saturates at large velocity at the highest allowable tilting where $\mathbf{V}_g$ is aligned on **a** [Figs. 4(c), 4(f), 4(i), and 4(l)]. Regarding asymmetry, it appears that the side towards which cells drift is flatter. This persists on dendrites and goes together with a larger sidebranching on the side opposite to the drift direction. This asymmetry gets more pronounced as Θ_0 or V_G increases and eventually yields secondary branches to nearly reach the tip isothermal line [Figs. 4(k) and 4(l)]. It then results in a larger distance between dendrite tips—i.e., a larger Λ—and thus a larger spatial period in the solid phase. On the other hand, one notices, at low V_G and large Θ_0, a transition to a so-called degenerate mode where two growth directions are simultaneously displayed together with tip splittings [Fig. 4(j)]. A remnant of this kind of dynamics persists a while on sidebranches when increasing velocity [Fig. 4(k)].

B. Qualitative evolution of growth direction

To better compare on a similar ground the evolutions of growth directions with the three variables (Θ_0, V_G, Λ), we report in Fig. 5 three sets of images referring, on each line, to an increase of one of these variables: V_G (first line), Λ (second line), or Θ_0 (third line). The other variables are otherwise kept constant except for Λ on the third line. Three vectors indicate on each snapshot the directions of **G**, **a**, and $\mathbf{V}_g$.

Increasing either V_G or Λ at otherwise fixed variables clearly yields a rotation of the growth direction $\mathbf{V}_g$ towards the direction **a** prescribed by the crystal orientation. As the misorientation angle Θ_0 was taken the same in these two

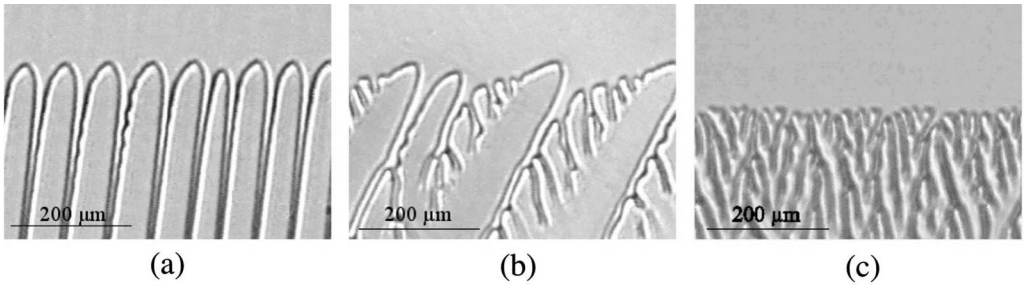

FIG. 6. Microstructure instabilities. (a) Elimination of the sixth cell from the left. (b) Creation of a dendrite from the growth of a secondary branch. (c) Degenerate mode.

series, the evolutions of the growth direction worth being qualitatively compared. They then appear somewhat similar for an increase of either V_G or Λ, in agreement with the identification of the Péclet number as a relevant variable of the issue [5] (Sec. V A). Increasing now the misorientation angle Θ_0 at fixed V_G and Λ also yields the growth direction to rotate, following the rotation of vector **a** with respect to **G**.

C. Microstructure instabilities

The different instabilities which bound the study are reported in Fig. 6. Two of them change the basic state by elimination [Fig. 6(a)] or creation [Fig. 6(b)] of a cell or a dendrite. The third instability maintains the interface in a permanent morphological evolution, the degenerate mode [Fig. 6(c)]. They are responsible for an absence of data at low Pe and large Θ_0.

Instabilities of elimination or of creation were encountered at too low or too large spacing, respectively [15]. Elimination results from the screening of the diffusion field by neighbors [Fig. 6(a)] and dendrite creation from the emergence of a secondary branch as an actual dendrite [Fig. 6(b)]. No oscillatory instability was noticed on cellular or dendritic patterns [16]. Finally, the degenerate mode made of iterative tip splittings prevented a definite growth direction from emerging [Fig. 6(c)]. It appeared at large $\Theta_0 > 35°$ for moderate Pe.

V. GROWTH DIRECTIONS, QUANTITATIVE ANALYSIS, AND SCALE INVARIANCE

We analyze the quantitative evolution of microstructure growth directions with (V_G, Λ, Θ_0). After having recovered the relevance of the Péclet number $\mathrm{Pe} = \Lambda V_G / D$, we evidence a scale invariance with respect to it from a collapse of data invariant by change of normalization. This property, confirmed in a log-log plot, enables the determination of the growth direction law.

A. Growth direction and Péclet number

In Sec. IV B, we noticed that the evolutions of growth directions with either velocity or spacing display the same kind of tendencies. This behavior is quantitatively confirmed in Fig. 7 at a misorientation angle of $\Theta_0 = 30.6°$: the growth direction angle Θ decreases with both the spacing Λ or the velocity V_G. The same conclusions is obtained at any Θ_0 in between 0° and 45°.

The similarity of the evolutions of Θ with either V_G or Λ suggests considering its dependence on the combined variable $\mathrm{Pe} = \Lambda V_G / D$ [5]. Figure 8(a) reports the dependence of Θ on Pe at three misorientation angles $\Theta_0 = 10.9°$, 30.6°, 39.7°. In agreement with the findings of Akamatsu and Ihle [5], a collapse of data $\Theta(\Theta_0, V_G, \Lambda)$ onto curves $\Theta(\Theta_0, \mathrm{Pe})$ is evidenced, whatever the values of V_G and Λ. Figure 8(b) shows that the same conclusion is achieved for any Θ_0. This confirms in the whole range $0° < \Theta_0 < 45°$ the similarity between V_G and Λ previously reported at $\Theta_0 \approx 30°$ (numerically and experimentally) and $\Theta_0 \approx 40°$ (experimentally) [5]. This result reduces the dependence of Θ to two variables only: Θ_0 and Pe.

B. Change of variable

To better compare the evolutions of growth directions with Pe at different Θ_0, it is convenient to absorb the differ-

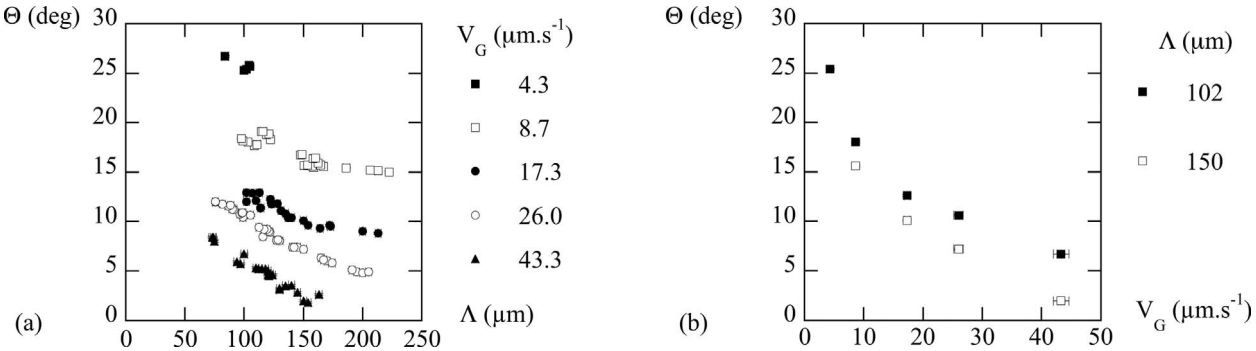

FIG. 7. Growth direction angle Θ as a function of the spacing Λ and the velocity V_G. The misorientation angle Θ_0 is fixed at $\Theta_0 = 30.6°$. (a) Θ as a function of Λ for five velocities V_G. (b) Θ as a function of V_G for two spacings Λ.

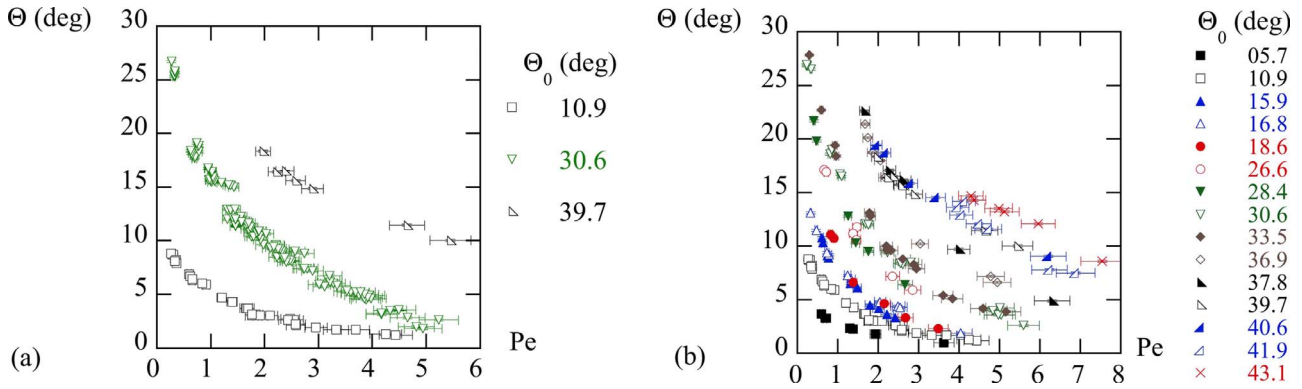

FIG. 8. (Color online) Collapse of data $\Theta(\Theta_0, V_G, \Lambda)$ onto a curve $\Theta(\Theta_0, \mathrm{Pe})$ (a) for three misorientation angles $\Theta_0 = 10.9°, 30.6°, 39.7°$ and (b) for any misorientation angle Θ_0 in our data range, $0° < \Theta_0 < 45°$.

ence in their limit values by considering the reduced growth angle Θ/Θ_0 [Fig. 9(a)]. The resulting curves differ depending on Θ_0, but nevertheless share common tendencies: all are monotonous and decreasing in between the same limit values. Moreover, their regular shapes show no characteristic Péclet number and no evidence of a transition to a different tendency at any Péclet number: no noticeable discontinuity of the curve, of its slope, or of its curvature and no repetitive feature.

These statements open the possibility of the absence of *any* characteristic Péclet number in this issue. This would correspond to a very specific feature, a scale invariance, which is known to largely restrain the possible forms of relationships [17]. To address its relevance here, we first seek to represent data in a way that treats the limit directions **G** and **a** symmetrically. This is not the case with the reduced variable Θ/Θ_0 since it expresses as the angle ratio $(\mathbf{a}, \mathbf{V}_g)/(\mathbf{a}, \mathbf{G})$ where **a** is taken as the sole reference of direction. To restore the expected symmetry, we thus introduce the relative angular position ξ defined as the ratio of angles $(\mathbf{V}_g, \mathbf{G})/(\mathbf{a}, \mathbf{V}_g)$:

$$\xi = \frac{(\mathbf{V}_g, \mathbf{G})}{(\mathbf{a}, \mathbf{V}_g)} = \frac{\Theta_0 - \Theta}{\Theta}. \quad (1)$$

The variable ξ now makes **G** and **a** play a similar role since both are taken as a direction of reference at the numerator or at the denominator. In particular, the permutation $\mathbf{a} \to \mathbf{G}$ is equivalent to the transformation $\xi \to \xi^{-1}$ which introduces no characteristic scale by its own [17]. This entails the fact that the variable ξ does not favor any scale from the way it is defined. In particular, its range of variation with Pe, $[0, \infty[$, displays no finite bound and thus no particular finite value [Fig. 9(b)]. It therefore appears suitable for addressing whether any characteristic scale is involved in the way $\mathbf{V}_g$ rotates from **G** to **a**.

C. Change of normalization

For functions of a *single* variable, the absence of characteristic scale selects a single family of solution: the power laws. In this case, the criterion for scale invariance then directly reduces to the relevance of power laws. However, here, the relative angular position ξ is a function of *both* Pe and Θ_0: $\xi \equiv \xi(\Theta_0, \mathrm{Pe})$. To test scale invariance with respect to Pe despite the dependence on Θ_0, it then appears convenient to return to the basic property of this symmetry: the invariance by change of scaling or, equivalently, of normalization factors. This consists in changing the standards implicitly used to evaluate Pe and ξ and probing this way the existence or the absence of a characteristic value of Pe or ξ.

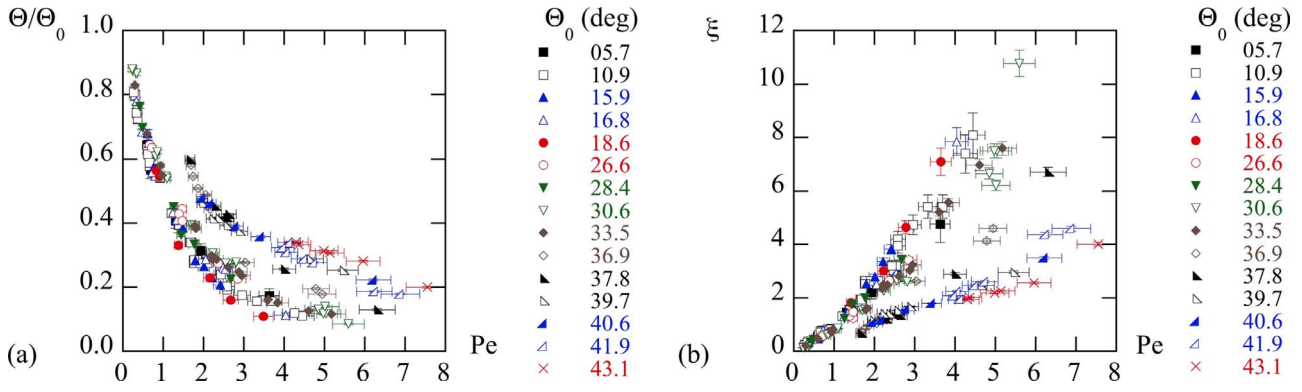

FIG. 9. (Color online) Different representations of data variation with Pe. (a) Reduced variables $(\Theta/\Theta_0, \mathrm{Pe})$. Although they undergo the same limits, curves differ depending on Θ_0. However, they display no characteristic Péclet number. (b) Variables suitable for the search for scale invariance: $\xi = (\Theta_0 - \Theta)/\Theta$ and Pe.

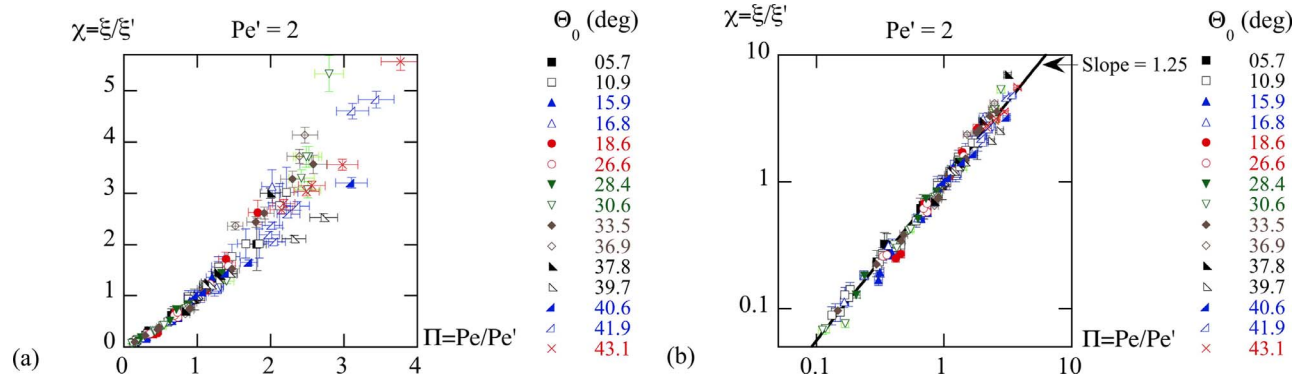

FIG. 10. (Color online) Evidence for scale invariance. (a) Normalized variables $\Pi=\mathrm{Pe}/\mathrm{Pe}'$, $\chi=\xi/\xi'$ using an arbitrary standard $\mathrm{Pe}'=2$ and $\xi'=\xi(\Theta_0,\mathrm{Pe}')$. Although $\chi(\Theta_0,\Pi,\mathrm{Pe}')$ *a priori* depends on three variables, data collapse on a curve in a (χ,Π) plot. The same collapse is obtained for other choices of Pe'. (b) Following (a), $\chi(\Pi)$ reduces to a single-variable scale invariant function—i.e., a power law. This is confirmed by the collapse on a line in logarithmic coordinates.

To apply this procedure appropriately, we link at each Θ_0 the normalizations on the ξ axis and on the Pe axis so that the point (1,1) belongs to the resulting curve. This corresponds to choosing, at each Θ_0, an *arbitrary* Péclet number Pe' as the standard of the Pe axis and the corresponding ξ value $\xi(\Theta_0,\mathrm{Pe}')=\xi'$ as the standard of the ξ axis, yielding the reduced variables

$$\chi=\frac{\xi(\Theta_0,\mathrm{Pe})}{\xi(\Theta_0,\mathrm{Pe}')},\quad \Pi=\frac{\mathrm{Pe}}{\mathrm{Pe}'}. \tag{2}$$

The variable χ then depends on Θ_0, Pe, and Pe' or, equivalently, on Θ_0, Π, and Pe'. It thus corresponds to a *three*-variable function $\chi(\Theta_0,\Pi,\mathrm{Pe}')$.

The procedure now consists, at each Θ_0, in changing the standard Pe' together with the coupled standard $\xi'=\xi(\Theta_0,\mathrm{Pe}')$ and in addressing the changes implied on the graphs of function $\chi(\Theta_0,\Pi,\mathrm{Pe}')$.

D. Scale invariance in Péclet number

As the function $\chi(\Theta_0,\Pi,\mathrm{Pe}')$ depends on three variables, its graph involves the four-dimensional space $(\chi,\Theta_0,\Pi,\mathrm{Pe}')$. Thus, projecting it onto the plane (χ,Π) should *a priori* yield a cloud of points. However, taking for Pe' an arbitrary common value, $\mathrm{Pe}'=2$, and for ξ' the interpolated value $\xi'=\xi(\Theta_0,2)$ yields in Fig. 10(a) a surprising collapse of data on a curve, whatever the values of Θ_0. A slight dispersion beyond error bars is only noticeable on fewer than a dozen points over more than 150—i.e. on less than 10% of the data. More than 90% of the data thus stand within one standard error from the collapse curve. This supports the statistical relevance of the collapse. In particular, scattering mostly addresses points for which ξ is the largest, and thus the implication of an uncertainty in ξ' is the biggest. It thus likely results from errors beyond the standard deviation in the determination of ξ'.

Here and above, the data error bars have been computed from the uncertainties of velocity $|\delta V_G|/V_G=|\delta V|/V=\pm 3\%$, spacing $|\delta\Lambda|=2000\ \mu\mathrm{m}/768$ with $\Lambda>70\ \mu\mathrm{m}$ and angles $|\delta\Theta|=|\delta\Theta_0|=0.1°$. They yield $|\delta\Pi|=0.07\Pi$, $|\delta\xi|=(0.1°/\Theta_0)(1+\xi)(1+2\xi)$, and $|\delta\chi|/\chi=|\delta\xi|/\xi+|\delta\xi'|/\xi'$.

The collapse of Fig. 10(a), which contrasts with the data spread of Fig. 9, is all the more surprising that the value chosen for the Péclet standard is arbitrary. This suggests that it should not refer to a coincidence, but rely on a deep property. To confirm this statement, we have applied the same procedure with different arbitrary choices of standard Péclet numbers: the maximal, minimal, and median Péclet numbers at each Θ_0. In each case, a collapse has again been evidenced and on the *same* curve within the experimental uncertainties.

These properties correspond to an invariance of function $\chi(\Theta_0,\Pi,\mathrm{Pe}')$ with respect to the choice of standards Pe' and to an independence with respect to Θ_0. The invariance with respect to Pe' reduces χ to a *two*-variable function $\chi(\Theta_0,\Pi)$ and states its scale invariance with respect to reduced Péclet numbers. The additional independence with respect to Θ_0 reduces χ to a *one*-variable function $\chi(\Pi)$, providing this way a surprisingly simple class of solutions to our issue.

E. Determination of the growth direction law

We exploit the scale invariance property to infer explicit information on the growth direction law.

1. Functional relationship and solution

As the function $\chi(\Theta_0,\Pi,\mathrm{Pe}')$ reduces to a single-variable function $\chi(\Pi)$, its scale invariance selects a power law. In the framework of a change of normalization, this follows from the fact that changing the standard Pe'_1 for a standard Pe'_2 changes $\Pi_1=\mathrm{Pe}/\mathrm{Pe}'_1$ into $\Pi_2=\mathrm{Pe}/\mathrm{Pe}'_2$ and $\chi_1=\xi/\xi'_1$ into $\chi_2=\xi/\xi'_2$ with $\xi'_1=\xi(\Theta_0,\mathrm{Pe}'_1)$ and $\xi'_2=\xi(\Theta_0,\mathrm{Pe}'_2)$. However, by definition of χ, one has

$$\chi_1(\Pi_1)=\frac{\xi(\Theta_0,\mathrm{Pe})}{\xi(\Theta_0,\mathrm{Pe}'_2)}\frac{\xi(\Theta_0,\mathrm{Pe}'_2)}{\xi(\Theta_0,\mathrm{Pe}'_1)}$$

or, equivalently, with $\mathrm{Pe}'_2/\mathrm{Pe}'_1=\Pi_1/\Pi_2$, $\chi_1(\Pi_1)=\chi_2(\Pi_2)\chi_1(\Pi_1/\Pi_2)$. Then, the invariance of the function $\chi(\Pi)$ by a change of the Péclet standard yields $\chi_1(\Pi)=\chi_2(\Pi)$ and thus a multiplicative relationship whose solutions, not everywhere discontinuous, are power laws [17]:

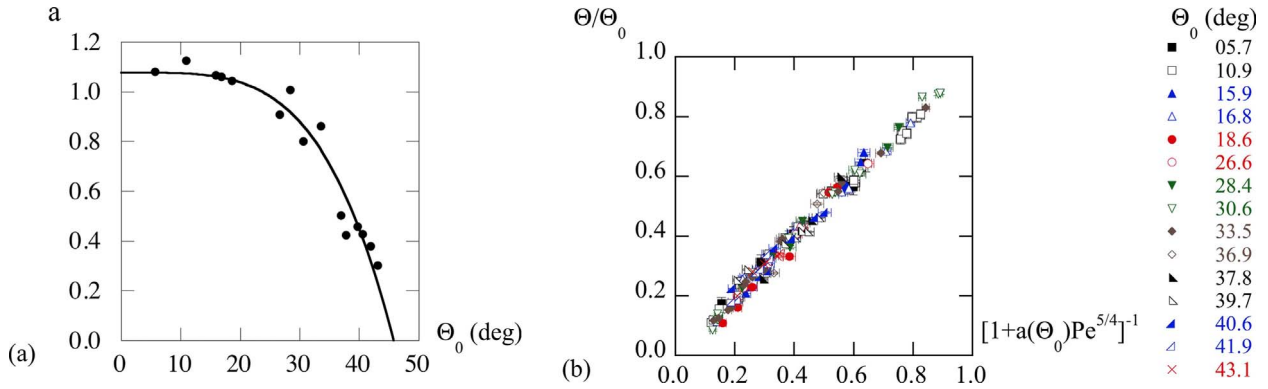

FIG. 11. (Color online) Determination of prefactors $a(\Theta_0)$ and test of the growth direction law (6) in our SCN alloy. (a) Values of $a(\Theta_0)$. The curve corresponds to the polynomial fit (5). (b) Ordinates correspond to Θ/Θ_0 and abcissa to $[1+a(\Theta_0)\mathrm{Pe}^{1.25}]^{-1}$.

$$\exists e; \quad \forall \Pi, \quad \chi(\Pi) = \Pi^e. \tag{3}$$

Interestingly, the independence of χ with respect to Θ_0 implies that the exponent e is a constant of the study.

The validity of the power-law relationship between χ and Π and its independence with respect to Θ_0 is confirmed in Fig. 10(b) by the collapse of all data on the same line in a log-log plot. Here, a Pe standard of 2 was used, but the same collapse on the same slope has been obtained for the other choices of arbitrary standards. Back to the function $\xi(\Theta_0,\mathrm{Pe})$, this implies $\xi(\Theta_0,\mathrm{Pe})=a(\Theta_0)\mathrm{Pe}^e$. Back to the growth angle Θ, this finally yields

$$\frac{\Theta}{\Theta_0} = \frac{1}{1 + a(\Theta_0)\mathrm{Pe}^e}. \tag{4}$$

2. Parameter determination

Fitting the whole data to relation (3) provides the value $e=1.249\pm0.004$, which we approximate to $e=1.25$. Then, at each Θ_0, the fit of data to relation (4) with $e=1.25$ provides the determination of prefactor $a(\Theta_0)$. The graph of a as a function of Θ_0 is reported in Fig. 11(a). It displays for $\Theta_0 < 25°$ some fluctuations around a plateau followed, are larger Θ_0, by a marked decrease towards zero. To empirically capture this tendency, we have fitted data with polynomials made by a constant term intended to represent the plateau and a single monomial intended to provide the shrinking to zero $P(\Theta)=\alpha[1-(\Theta/\Theta_m)^\beta]$. The best adjustment is obtained for $\alpha=1.08$, $\beta=4$, and $\Theta_m=45.8°$ with a satisfactory agreement [Fig. 11(a)]. It corresponds to the following parametrization:

$$a(\Theta_0) = 1.08\left[1 - \left(\frac{\Theta_0}{45.8°}\right)^4\right]. \tag{5}$$

3. Growth direction law

Altogether, relation (4) and the identification of parameters e and $a(\Theta_0)$ yield the following determination of the growth direction law in our mixture:

$$\frac{\Theta}{\Theta_0} = \frac{1}{1 + 1.08\left[1 - \left(\frac{\Theta_0}{45.8°}\right)^4\right]\mathrm{Pe}^{1.25}}. \tag{6}$$

It is made of an algebraic form (4) linked to an internal symmetry (3) and of an empirical determination (5) of the effect of Θ_0. The plot of our data in coordinates corresponding to both members of relation (6)—i.e. $y=\Theta/\Theta_0$ and $x=[1+a(\Theta_0)\mathrm{Pe}^{1.25}]^{-1}$—makes them collapse on the first bisector $y=x$ [Fig. 11(b)]. This quantitative agreement validates the family of solutions (4) and the determination of its parameters e and a.

VI. DISCUSSION

A. Structure of the growth direction law

1. Internal symmetry and physical equivalence

The existence of an internal symmetry, the Péclet scale invariance, brings about deep implications on the way the evolution of microstructure growth directions must be conceived. The main property attached to this symmetry states that the relative increase of angle ratios $\xi(\mathrm{Pe}_2)/\xi(\mathrm{Pe}_1)$ between two Péclet numbers only depends on the relative Péclet increase $\mathrm{Pe}_2/\mathrm{Pe}_1$ *independently* of the absolute Péclet values Pe_1 or Pe_2. This formally means that the relative increase $\xi(\mathrm{Pe}_2)/\xi(\mathrm{Pe}_1)=\chi(\mathrm{Pe}_1,\mathrm{Pe}_2/\mathrm{Pe}_1)$, which *a priori* depends on the two variables Pe_1 and $\mathrm{Pe}_2/\mathrm{Pe}_1$, actually only depends on the latter: $(\partial\chi/\partial\mathrm{Pe}_1)_{\mathrm{Pe}_2/\mathrm{Pe}_1}=0$.

This property destroys the relevance of the concept of large or small Péclet number. In particular, *all* Péclet numbers except 0 and ∞, *all* growth directions except the asymptotical ones **G** and **a**, *all* misorientation angles, and thus *all* states of Figs. 4 or 5 are *physically equivalent* regarding the evolution of growth directions, in the sense that the relative increase of angular position ξ is *independent* of their absolute value or of their absolute state. It thus refers to the same kind of issue for all and has, therefore, the same kind of answer for all.

This statement is actually surprising owing to the large morphological differences displayed by microstructures (Figs. 4 and 5). It however states that, for understanding the

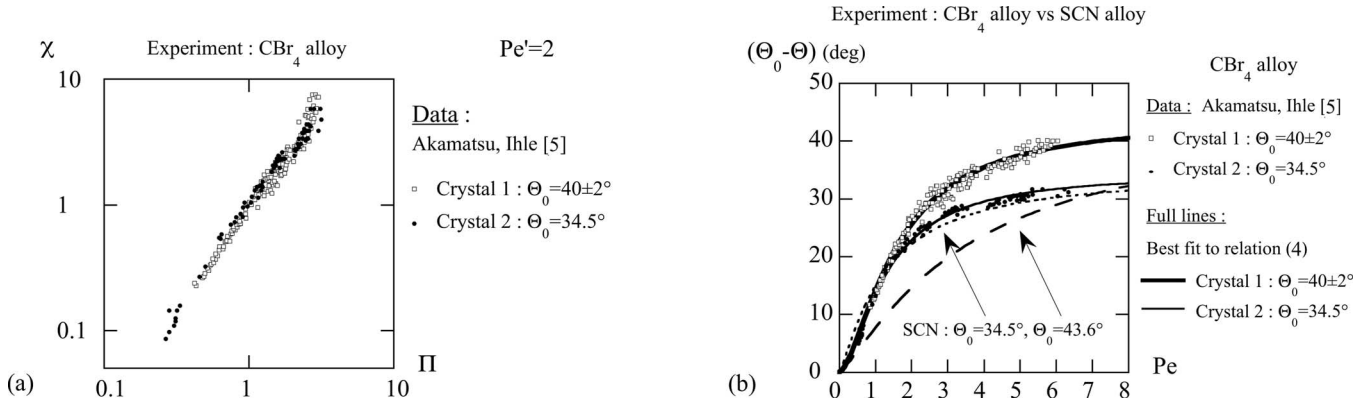

FIG. 12. Experimental data in a CBr_4 alloy [5]. (a) Evidence of Péclet scale invariance in logarithmic coordinates (χ,Π). (b) Original variables $(\Theta_0-\Theta,\mathrm{Pe})$ of Ref. [5]. Fit to the growth direction law (4) and comparison with our SCN alloy.

origin of the scale invariant growth direction law, one may equally choose to focus attention on small misorientation angles Θ_0 instead of on large ones, on cells or weakly branched dendrites instead of on well-developed dendrites, and on low Péclet numbers instead of on large ones.

This degree of freedom brought about by scale invariance might be convenient in numerical simulations or theoretical analyses to avoid useless complexity. More generally, it would also be valuable to test its validity on other important features such as the tip undercooling [18] for achieving a deeper understanding of the role of crystal anisotropy in solidification.

2. Similarity versus scale invariance

Two kinds of properties altogether give rise to the growth direction law (4). One refers to the similarity between variables V_G and Λ, the other to the scale invariance with respect to the Péclet number. Both largely differ regarding their meaning and their implications.

Similarity points to the combined variable $\mathrm{Pe}=\Lambda V_G/D$ as a relevant variable of the issue. However, by itself, the role of this variable is no surprise, since the issue can be considered in terms of nondimensional variables including Pe. The actual information is thus on the *absence* of a noticeable *variation* of Θ on the remaining nondimensional variables that involve V_G and Λ: V_G/V_c and Λ/d_0.

Similarity therefore denies *relevance* to some combined variables. In contrast, scale invariance deals with the *remaining* ones by stating the *absence* of *preferred values* for them. It thus states the physical equivalence of all their magnitudes, no matter large or small. Interestingly, this selects a definite structure (3) and (4) for the corresponding law.

3. Prefactor dependence on Θ_0

The dependence of prefactor a on Θ_0 in relation (5) is responsible for a nonlinear evolution of Θ with Θ_0 at fixed Pe. This nonlinearity was noticed in simulations at $\mathrm{Pe}=2.758$ [6] and $\mathrm{Pe}=2.925$ [5] and is attested to here on all Péclet numbers [Fig. 11(b)]. However, in contrast with the power-law dependence (3) which relies on a fundamental symmetry, the dependence of a on Θ_0 is only empirical and calls to be clarified.

B. Comparison to previous studies

1. Experimental studies

A single previous experimental study—that of Akamatsu and Ihle in a CBr_4–C_2Cl_6 alloy [5]—has provided data suitable for a comparison with our findings. Two misorientation angles were studied in two single crystals named crystals 1 and 2. Figure 12(b) reproduces the original data of this study which express the growth angle $(\mathbf{V}_g,\mathbf{G})=(\Theta_0-\Theta)$ as a function of Pe. The two angles Θ_0 were not directly measured, but later evaluated from the asymptote (crystal 1, $\Theta_0=40°\pm2°$; crystal 2, $\Theta_0=32°\pm2°$). However, a comparison with a numerical simulation performed at $\Theta_0=30°$ led to a more accurate determination in crystal 2, $\Theta_0=34.5°$, which we shall retain from now on.

Computing the reduced variables (χ,Π) for a standard Péclet number $\mathrm{Pe}'=2$ yields evidence of a fine collapse on a line in logarithmic coordinates [Fig. 12(a)]. This extends the validity of the Péclet scale invariance to this experiment. The fits to relation (4) are displayed in Fig. 12(b) in the original variables of the experiment. They confirm the relevance of the growth direction law with the following exponents $e=1.60\pm0.05$ in crystal 1 and $e=1.61\pm0.03$ in crystal 2. Adopting a common value of 1.60 for both, another fit gives $\Theta_0=43.6\pm0.2°$ and $a=0.47\pm0.01$ for crystal 1 and $a=0.64\pm0.01$ with Θ_0 fixed at 34.5° for crystal 2.

The variation of parameter a in crystals 1 and 2 means that each angle Θ_0 brings about a specific response. Additional data are thus required to clarify the evolution of $a(\Theta_0)$ and thus of growth directions in this alloy.

For comparison, the evolution of growth directions in our SCN alloy are plotted on the same graph for the same misorientation angles $\Theta_0=43.6°$ (dashed line) and $\Theta_0=34.5°$ (dotted line). They largely differ from those displayed in the CBr4 alloy for $\Theta_0=43.6°$, but are close to them for $\Theta_0=34.5°$. This shows that the way growth directions depend on Θ_0 may largely change with the nature of the melt so that no extrapolation can apparently be made from one material to the other. This supports the need for additional data in CBr_4 alloys.

The closeness of the data referring to the two alloys for $\Theta_0=34.5°$ is surprising in view of the difference between the

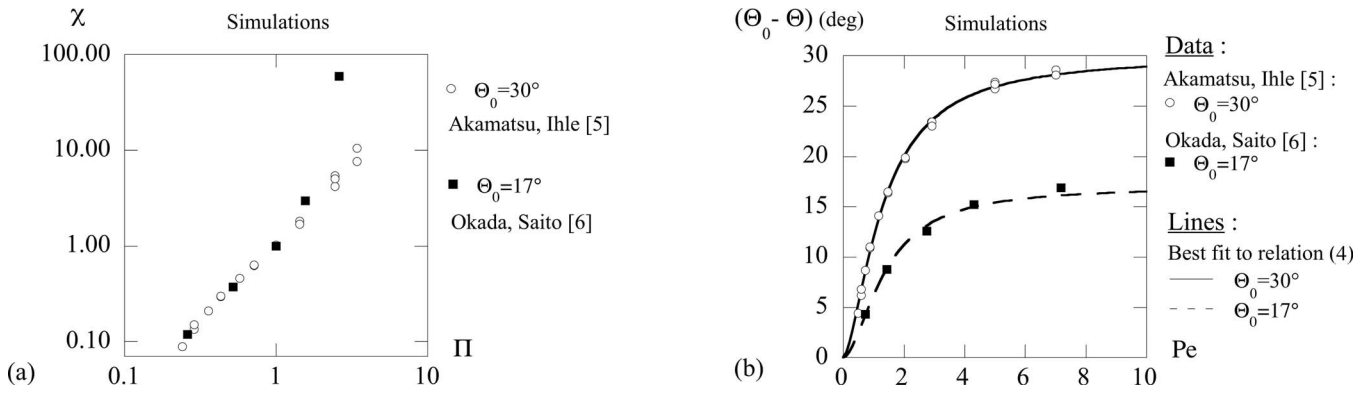

FIG. 13. Numerical simulations [5,6]. (a) Evidence of Péclet scale invariance in logarithmic coordinates (χ,Π). (b) Original variables $(\Theta_0-\Theta,\mathrm{Pe})$ of Refs. [5,6] and fit to the growth direction law (4).

parameters of their growth direction law: $(e,a)=(1.60,0.64)$ for the CBr_4 alloy and $(e,a)=(1.25,0.75)$ for the SCN alloy. It means that the change induced in relation (4) by the variation of e from 1.60 to 1.25 at *fixed* a is largely reduced by a *simultaneous* variation of a from 0.64 to 0.75. This may go together with a low standard error for the fit parameters since standard errors address the confidence in best fit values in view of data scattering whereas the above remark addresses the variation of the fit function with its parameters. The possible weak variation of this function for coupled changes of e and a, however, stresses that additional data at other Θ_0 could noticeably change the value of a best fitting parameter. Further investigations at other misorientation angles Θ_0 are thus necessary to firmly conclude about the value of e in CBr_4 alloys and more generally about an actual variation of exponents with alloys.

2. Numerical studies

Two numerical simulations of growth directions have been worked out in directional solidification. One, by Okada and Saito was intended to simulate the solidification of steel with impurities of Cr and Ni [6]. The other, by Akamatsu and Ihle, was designed to mimic solidification in CBr_4—C_2Cl_6 alloys [5]. The former involved a surface tension anisotropy and no kinetic anisotropy, whereas the latter involved both. Both simulations considered a single misorientation angle $\Theta_0=17°$ [6] and $\Theta_0=30°$ [5].

Variables $\chi(\Pi)$ are computed for both simulations using the following standards: $(\mathrm{Pe}',\xi')=(2.04,1.94)$ for Ref. [5] and $(\mathrm{Pe}',\xi')=(2.76,2.86)$ for Ref. [6]. They both yield in Fig. 13(a) a collapse on a line in logarithmic coordinates except for the highest Pe data in Ref. [6]. This extends the relevance of the Péclet scale invariance to these simulations. Confirmation of the relevance of the growth direction law (4) is shown in Fig. 13(b) in the original variable $(\Theta_0-\Theta)$ of the simulations. It corresponds to the following best fitting parameters: $(e,a)=(1.75\pm0.16,0.57\pm0.05)$ with $\Theta_0=17°$ for Ref. [6] and $(e,a)=(1.60\pm0.04,0.66\pm0.01)$ with $\Theta_0=30°$ for Ref. [5].

3. Nonlinearity of the variation with Θ_0 at fixed Pe

At fixed Péclet number, the evolution of Θ with Θ_0 evidences the deviation from linearity implied by the variation of parameter a with Θ_0, Eq. (4). It has been determined in numerical simulation at $\mathrm{Pe}=2.758$ [6] and $\mathrm{Pe}=2.925$ [5] and can be obtained in our SCN mixture at any Péclet number—e.g., $\mathrm{Pe}=2.925$ here—using the growth direction law (6). Figure 14 shows a larger nonlinearity in both our mixture and the simulations of Okada and Saito. In addition, the departure from linearity begins first in the simulation of Okada and Saito ($\Theta_0\approx25°$) [6], then in our SCN mixture ($\Theta_0\approx30°$), and finally in the simulation of Akamatsu and Ihle ($\Theta_0\approx35°$) [5]. Interestingly, this order corresponds to increasing the kinetic interfacial anisotropy (from zero [6] to a small value in our SCN mixture and a noticeable one, $\epsilon_k=12\%$ [5]), but to decreasing the interfacial stiffness anisotropy coefficient (from 10% [6] to 8% in our mixture and 6% [5]). Other studies are thus required to clarify the implication of interfacial anisotropy on the nonlinearity of the growth direction evolutions.

VII. CONCLUSION

In casting and directional solidification, the growth directions of cellular or dendritic microstructures with respect to the melt stand in between the heat flow direction and a preferred crystalline orientation. As the solidification velocity increases, the growth direction is found to rotate from the former to the latter, with important implications regarding

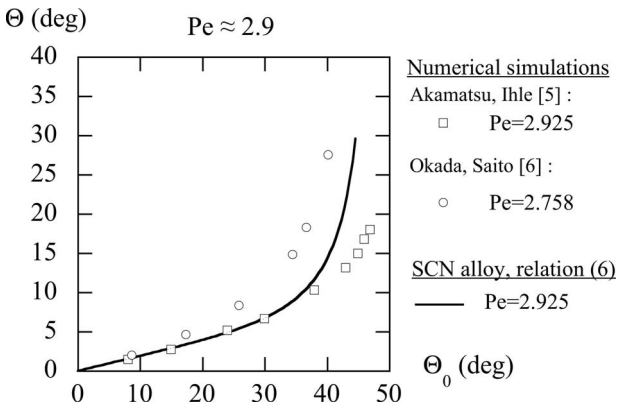

FIG. 14. Nonlinear evolution of Θ with Θ_0 at fixed Pe.

the microstructure morphology and thus the microsegregation of the resulting material. Here, we have documented in detail this evolution in a thin sample experiment involving a single cubic crystal with one principal axis normal to the sample plane. Our data library extends over 15 misorientation angles Θ_0 between thermal gradient and preferred crystalline direction and, for each, on about 10 solidification velocity V_G or microstructure spacings Λ. This provides the largest data library obtained on this issue to date.

Data analysis confirm the relevance of the Péclet number $\mathrm{Pe}=\Lambda V_G/D$ to handle the similarity between the variations of growth directions implied by V_G or Λ. Deeply analyzing their nature, we have evidenced from a data collapse an unexpected symmetry shared by all of them: a scale invariance with respect to the Péclet number. This symmetry denies the existence of any preferred value of Pe in the evolution of growth directions. It thus surprisingly states that all growth states are physically equivalent regarding the implications of a Péclet increase on growth directions, no matter whether the tilt angle is large or small, the asymetry pronounced or faint, and the sidebranching developed or weak (Figs. 4 and 5).

This Péclet scale invariance led to the identification of the structure of the growth direction law. The dependence with respect to Θ_0 then appeared to be handled in a single parameter $a(\Theta_0)$ displaying a continuous variation on the whole accessible range. This supports the existence of a single physical regime, referring to a deep symmetry in this issue. In addition, the relevance of the Péclet scale invariance appeared to extend to previous quantitative experiments and simulations [5,6] with different determinations of exponents and prefactors.

These results raise several open questions that need to be addressed before reaching a satisfactory understanding of the growth directions of microstructures. The first questions refer to the origins of the similarity (i.e., the absence of dependence on some nondimensional variables) and of the Péclet scale invariance (i.e., the irrelevance of the magnitude of Péclet numbers for the evolution of growth directions). The second important issue refers to the origin and the nature of the parameter $a(\Theta_0)$ which drives the variation of growth directions with respect to Θ_0. All call for investigating the orientational response of microstructures in different materials so as to quantitatively address the influence of anisotropic modulations of surface tension or of kinetic undercooling. Finally, it will be worth investigating the implications on growth directions of inhomogeneities of microstructure patterns (e.g., cellular or dendritic spacing), of thermal gradient distortion (e.g., curved isothermal lines [19]), or of crystal orientation (e.g., multigrains). This would offer the opportunity of going closer to actual casting conditions so as to transfer to practical situations the findings evidenced here on single crystals confined in thin samples.

ACKNOWLEDGMENTS

We thank S. Bodea for stimulating discussions and J. Minelli for technical assistance.

[1] B. Chalmers, *Principles of Solidification* (Wiley, New York, 1964); M. C. Flemings, *Solidification Processing* (McGraw-Hill, New York, 1974); W. Kurz and D. J. Fischer, *Fundamentals of solidification* (Trans tech Publications, Zurich, 1984); W. J. Boettinger, S. R. Coriell, A. L. Greer, A. Karma, W. Kurz, M. Rappaz, and R. Trivedi, Acta Mater. **200**, 43 (2000).

[2] A. G. Borisov, O. P. Fedorov, and V. V. Maslov, J. Cryst. Growth **112**, 463 (1991); O. P. Fedorov, *ibid.* **156**, 473 (1995); G. He, J. Li, X. Mao, and H. Fu, J. Mater. Sci. Technol. **14**, 200 (1998); G. L. Ding and S. N. Tewari, J. Cryst. Growth **236**, 420 (2002).

[3] R. Trivedi, Appl. Mech. Rev. **43**, 79 (1990); R. Trivedi, V. Seetharaman, and M. A. Eshelman, Metall. Trans. A **22**, 585 (1991).

[4] P. Oswald, M. Moulin, P. Metz, J. C. Géminard, P. Sotta and L. Sallen, J. Phys. III **3**, 1891 (1993).

[5] S. Akamatsu and T. Ihle, Phys. Rev. E **56**, 4479 (1997).

[6] T. Okada and Y. Saito, Phys. Rev. E **54**, 650 (1996).

[7] J. Deschamps, M. Georgelin, and A. Pocheau, Europhys. Lett. **76**, 291 (2006); A. Pocheau, J. Deschamps, and M. Georgelin, JOM **59**, 71 (2007).

[8] T. Haxhimali, A. Karma, F. Gonzales, and M. Rappaz, Nat. Mater. **5**, 660 (2006).

[9] J. D. Hunt, K. A. Jackson, and H. Brown, Rev. Sci. Instrum. **37**, 805 (1966).

[10] M. Georgelin and A. Pocheau, Phys. Rev. E **57**, 3189 (1998).

[11] S. R. Coriell and R. F. Sekerka, J. Cryst. Growth **34**, 157 (1976).

[12] G. W. Young, S. H. Davis, and H. Brattkus, J. Cryst. Growth **83**, 560 (1987).

[13] A. Pocheau and M. Georgelin, Phys. Rev. E **73**, 011604 (2006).

[14] S. Akamatsu, G. Faivre, and T. Ihle, Phys. Rev. E **51**, 4751 (1995).

[15] A. Pocheau and M. Georgelin, J. Phys. IV **11**, 169 (2001).

[16] M. Georgelin and A. Pocheau, Phys. Rev. Lett. **79**, 2698 (1997).

[17] G. I. Barenblatt, *Similarity, Self-similarity and Intermediate Asymptotics* (Consultants Bureau, New York ,1996); L. I. Sedov, *Similarity and Dimensional Methods in Mechanics* (CRC Press, Boca Raton, 1993); A. Pocheau, Phys. Rev. E **49**, 1109 (1994); Eur. Phys. J. B **49**, 491 (2006).

[18] T. F. Bower, H. D. Brody, and M. C. Flemings, Trans. Metall. Soc. AIME **236**, 624 (1966); A. Pocheau and M. Georgelin, J. Cryst. Growth **206**, 215 (1999).

[19] S. Bottin-Rousseau and A. Pocheau, Phys. Rev. Lett. **87**, 076101 (2001); A. Pocheau and S. Bottin-Rousseau, Chaos **14**, 882 (2004).